Indian Journal of Pure & Applied Physics
Vol. 54, May 2016, pp. 301-306

Effect of uniform helium doping on the optical properties and laser damage performance of sapphire

M Zhong[1], X Xiang[1]*, W Liao[2], Z H Yan[1], L Yang[1], G X Yang[3], J W WU[1], W G Zheng[2] & X D Yuan[2]

[1]School of Physical Electronics, University of Electronic Science and Technology of China, Chengdu 610054, China

[2]Research Center of Laser Fusion, China Academy of Engineering Physics, Mianyang 621900, China

[3]Institute of Nuclear Physics and Chemistry, China Academy of Engineering Physics, Miangyang 621900, China

Received 10 June 2015; revised 15 December 2015; accepted 6 January 2016

Sapphire samples have been implanted successively by helium ions with a series of energies to obtain a uniform layer of impurities in the range of 80-200 nm beneath the surface at room temperature. After helium ion implantation, the surface morphology has been greatly changed. In addition, two broad absorption bands at 360 nm and 780 nm are observed and their intensities significantly increase. An infrared band shifts from 782 cm^{-1} to 760 cm^{-1} and the band obviously broadens. Moreover, a luminescence band at 330 nm (3.8 eV) is associated with the 2P→1S* transition of the F^+ centers. After laser irradiation, the laser damage morphologies of samples before and after ion implantation are presented. An obvious degradation of laser induced damage threshold (LIDT) is observed and the mechanism for the degradation of LIDT is discussed.

Keywords: Sapphire, He ions implantation, absorption, luminescence, LIDT

1. Introduction

Sapphire have been widely used in several technological applications due to its interesting properties such as high melting point and high temperature insulator and radiation-resistance material[1]. In addition, sapphire is proved candidate for using in fusion reactors as an insulator and for optical windows because of its good radiation-resistance performance[2]. In the fusion devices, nuclear and laser application, sapphire as well as other optical materials such as fused silica[3,4] and KDP[5] will be subjected not only to neutron and gamma irradiation, but also to energetic particles bombardment such as helium ions, due to ionization of the residual gas and acceleration of the resulting ions by local electric fields[6]. Therefore, the optical materials will be inevitably damaged and their microstructures and optical properties as well as laser damage resistance will change. With the wide and further application of fusion and laser, it is of importance to investigate the defects and damages in sapphire generated by radiation. Thus, numerous studies on the radiation damage mechanisms of sapphire produced by irradiation have been studied[7]. In modern technology and practice engineering, the irradiation problem of optical materials will still face a huge challenge.

On the other hand, ion implantation as a mature technique is not only used for surface modification, but also can improve the understanding of defect evolution. It shows potential promise as a means of modifying the near-surface mechanical, electrical, optical, and magnetic properties in sapphire matrices[8-11]. In general, the depth of implantation is totally dependent on the implanted energy, while the amount of implantation is defined by the implantation fluence. However, it will be saturated when the impurity concentration reaches a certain value and above. Based on the results of SRIM (the Stopping and Range of Ion in Matter) code[12], the depth profile of implantation is a Gaussian distribution with projected range near to the surface of material. The SRIM is used to calculate many features of the transport of ions in matter. Its typical applications mainly include: ion stopping and range in targets, ion implantation, sputtering and ion transmission. For some optical devices, the ion beams may require different energies in order to obtain a layer of special impurity beneath the surface in some cases. It is presented that helium ion-beam, using a series of energies to produce a continuous damage, has been used to generate severe lattice damage for fabricating three-dimensional structures such as channels and bridges in sapphire[13]. It is interesting that a uniform and stable layer of implantation ions can be obtained by using a series of different energies to implant.

*Corresponding author (E-mail: xiaxiang@uestc.edu.cn)

For He^+ ion beam implantation, the effects of He implanted sapphire have been investigated such as optical property[2,7], electrical property[14], and microstructure evolution[15-17]. The damage evolution, dislocation loops and bubbles in sapphire implanted with 10 keV over the temperature range of room temperature to 1000°C has been observed by an electron microscope[17]. In addition, 30 keV energy He ions irradiation with four different fluences of 0.1, 0.3, 1.0 and 2.0×10^{16} ions/cm^2 has been investigated[16]. In-situ analysis of ion-induced luminescence of sapphire by He ions implantation with 30 keV energy and the fluence up to 2.0×10^{16} ions/cm^2 have been performed[2]. Moreover, the effect of surface optical and electrical degradation have also been studied by 54 keV He ions implantation up to a dose of 10^{17} ions/cm^2 at 50, 250 and 450°C, respectively[14]. However, to our knowledge, there has been no report about the effect of ion beam implantation on the laser damage resistance of sapphire. Therefore, the optical properties and microstructure evolution as well as the LIDT of helium ion implanted sapphire is investigated in this work.

2. Experimental Procedure

To obtain a uniform layer of He ions in sapphire substrate, a simulation calculation is carried out. For calculation, the density of sapphire is 3.98 g/cm^3 and the displacement energy of 20 eV and 50 eV is used for Al and O atoms, respectively[18]. The SRIM calculation result of He implanted sapphire with a series of energies is shown in Fig.1. It is clearly revealed that there has a uniform layer of He impurity in the range of 80-200 nm beneath the surface. The maximum of helium concentration is about 2.0×10^{22} He^+/cm^3.

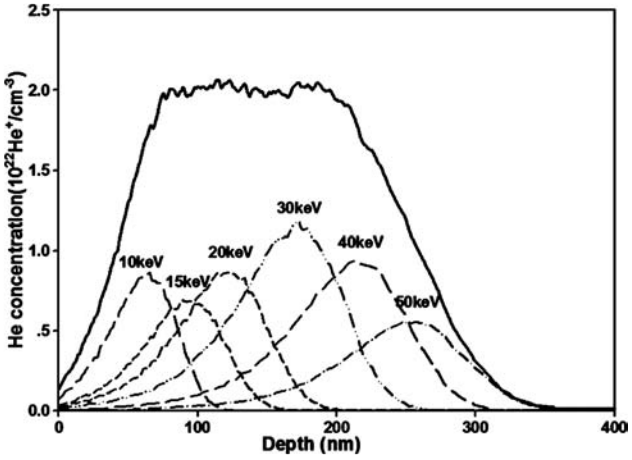

Fig. 1 – SRIM calculation of He implanted sapphire with a series of energies

In the present work, the (001)-orientated sapphire samples with two-side optical polishing were used and the sizes of samples were 10 mm × 10 mm × 0.5 mm. Before the experiment, all of samples are repeatedly cleaned by using sulfuric acid and ultrasonic to remove the residual abrasive compound. Some samples were successively implanted by helium ions with a series of energies of 10, 15, 20, 30, 40, and 50 keV at nominal fluences of 5×10^{16}, 6×10^{16}, 7×10^{16}, 1.1×10^{17}, 9.5×10^{16} and 6×10^{16} ions/cm^2 at room temperature, respectively. The pristine sapphire was used as a reference. The ion beam current density was controlled at 17 μA/cm^2. The angle between incident beam and the main crystallographic directions of sapphire is about 7^o to avoid the channeling effects during the implantation process. A Nikon PSIA XE-100 atomic force microscope (AFM) and A FEI Helios Nanolab 650 scanning electron microscope (SEM) operating at 30 kV with current of 0.4 nA were utilized to observe the surface morphology of samples before and after helium ions implantation. The optical absorption measurements were carried out by using a Perkin-Elmer Lambda 950 UV-vis-NIR spectrophotometer in the wavelength range 200-2500 nm. The infrared (IR) spectra were collected by a Nicolet 950 FTIR spectrometer. The photoluminescence (PL) spectra were obtained by a Perkin-Elmer LS55 fluorescence spectrometer. All of the characterizations were operated at room temperature.

In order to understand the laser damage resistance capability of optical materials used for laser facilities, the LIDT was tested with R-on-1 procedure[19] (multiple shots of increasing laser fluence at a single site of the material) before and after ion implantation, i.e., the laser fluence used for irradiating the material is increased at a fixed step until damage is observed. The LIDT tests were conducted by using a mono-longitudinal mode Nd:YAG pulse laser operated at 355 nm with a pulse length of 6.4 ns. The laser-shot interval in R-on-1 damage testing is several seconds. The laser beam was a spatial near-Gaussian distribution with beam area of 1 mm^2 at 1/e^2. The beam areas were observed by a science CCD camera to monitor the initial damage in several microns in the surface of sapphire samples. The laser fluence fluctuates less than 5%. An EMP 1000 energy meter was used to collect the energy data of each shot. A Nikon ECLIPSE LV100 optical microscope was used to observe the laser damage morphologies of the

samples. The depth profile of the damage morphology was measured by a Dektak 150 profilometer.

3. Results and Discussion

3.1 Microstructure evolution

In order to investigate the process of microstructure evolution in sapphire, the surface morphologies have been measured with AFM and SEM. The AFM images of pristine and He implanted sapphire are shown in Fig. 2. After comparing Fig. 2(a) and 2(b), it can be seen that it has a great change occurs on the surface of the samples where the root mean square (RMS) roughness is 0.515 nm and 1.561 nm, respectively. It indicates that there has obvious effect on the surface after helium implantation with a series of energies. It is shown that the changes of the samples surface are probably due to the aggregation of defects induced by ion implantation.

The SEM images of pristine and He implanted sapphire are shown in Fig. 3. It is clearly shown in Fig. 3(a) that the surface of the pristine sample is smooth and uniform. However, a very rough surface with a large number of bulges on the He-implanted sample is observed from Fig. 3 (b). The helium bubbles formed and then released from the surface should be responsible for the rough surface after ion implantation. The bubble concentration inside the ion implantation layer has been approximately estimated and the pressure in the bubbles is inversely proportional to the size of the bubbles[16]. Therefore, under the lateral stress and gas pressure, the bubbles will swell and remove near to the surface in the sapphire during the ion implantation process. Moreover, the high concentration of defects, produced by helium ions implantation, will favor the aggregation of associated defects[11]. According to the previous findings, it is reasonably concluded that the rough surface is probably due to the aggregation of defects induced by ion implantation and helium bubbles swelling and then release from the surface.

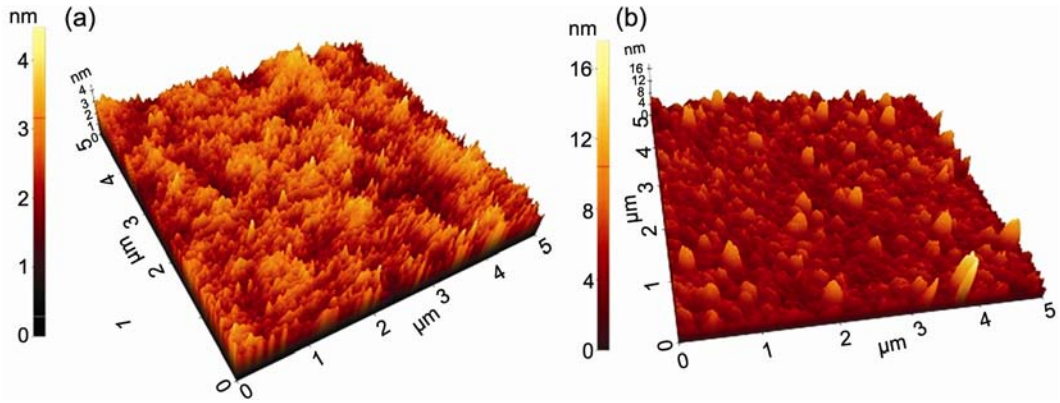

Fig. 2 – AFM images of (a) pristine and (b)He implanted sapphire

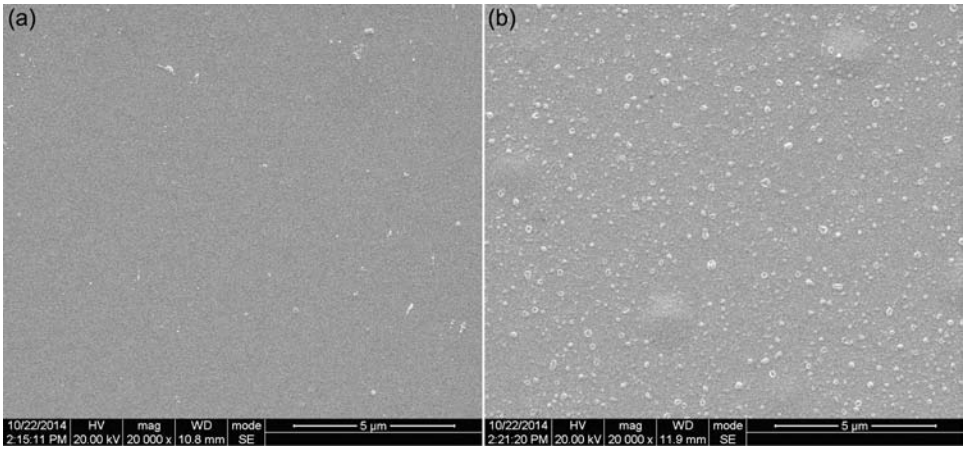

Fig. 3 – SEM images of (a) pristine and (b)He implanted sapphire

3.2 Optical properties

To investigate the optical property of sapphire before and after He ions implantation, the optical absorption spectra in the UV-vis-NIR and IR spectra as well as PL spectra in the UV-vis wavebands are investigated. The UV-vis-NIR optical absorption of He implanted sapphire with a series of energies is illustrated in Fig. 4. It is clearly shown that two broad absorption bands at 360 nm and 780 nm are observed and their intensities increase greatly after helium implantation. In fact, the absorbance data in this work includes scattering. It is difficult to distinguish precisely between absorbance and scattering. The absorption band at 360 nm is assigned to the aggregate oxygen vacancies in the form of dimer F_2^+ centers (two oxygen vacancies trapping three electrons)[20]. It is suggested that the 780 nm color center may be identified as (Al-O^-) intrinsic defect, which cannot be ruled out that Al-O-Al bond breaking[21].

The IR spectra of helium implanted sapphire are shown in Fig. 5. The inset shows the IR spectra in the range of 650-1000 cm^{-1}. It is obviously revealed from the inset that there are two interesting phenomena: peak shift and broadening. There is an original strong IR band at 782 cm^{-1} in the pristine sample, which is assigned to valence vibration of bonds Al-O[22]. There is an IR shift occurs after ion implantation from 782 cm^{-1} to 760 cm^{-1}, which is probably due to lattice distortions. In addition, the band peak has been broadened after ion implantation, which is probably contributed to the defects induced by helium ions implantation.

To understand the luminescence properties of sapphire after implanting a uniform layer of He impurities, the PL spectra are investigated. The PL spectra of He implanted sapphire excited by 225 nm are shown in Fig. 6. It is clearly revealed that there are two obvious bands at 330 nm and 660 nm after He ions implantation. The band at 330 nm (3.8 eV) is ascribed to the F^+ center (an oxygen vacancy with one trapped electron) whereas the 660 nm is attributed to the second-order structure of the main peak at 330 nm.[7] Furthermore, the 3.8 eV luminescence band is associated with the 2P→1S* transition of the F^+ center[23,24]. In addition, the inset is the emission spectra of He implanted sapphire excited by 330 nm. It clearly turns out that the two emission bands centered at 225 nm (5.4 eV) and 255 nm (4.8 eV) are both ascribed to F^+ centers, which are assigned to the 1A→1B and 1A→2A transitions of the F^+ centers [23].

3.3 Laser radiation

In this work, A is defined as the maximum laser fluence before the material is damaged and B is

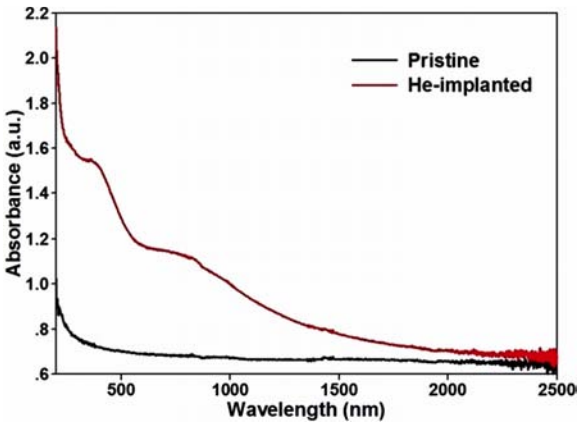

Fig. 4 – UV-vis-NIR optical absorption of He implanted sapphire

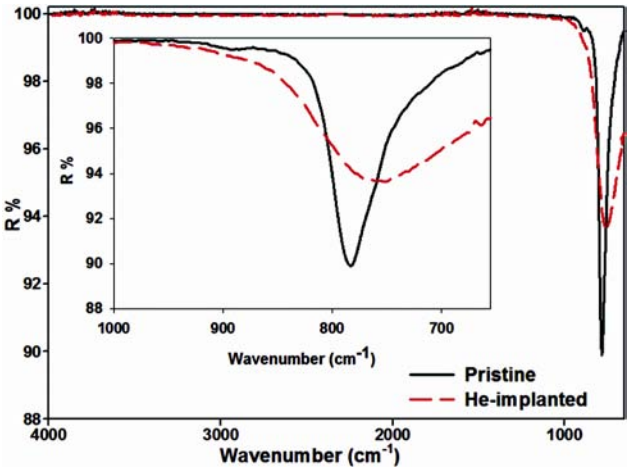

Fig. 5 – IR spectra of He implanted sapphire

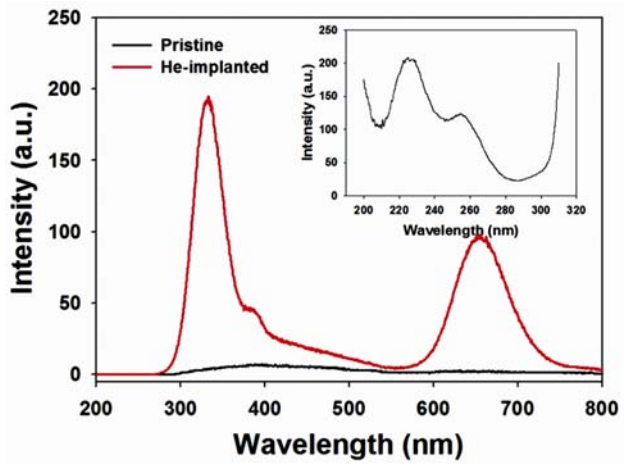

Fig. 6 – PL spectra of He implanted sapphire excited by 225 nm

defined as the laser fluence when damage just occurs. So the LIDT is expressed as LIDT= (A+B)/2 and Error = (B-A)/2. The distribution of LIDTs before and after He implanted sapphire is illustrated in Fig. 7. It is clearly shown that the LIDTs decrease greatly after helium implantation. The average LIDT of the pristine and the He-implanted sample are 5.33 J/cm^2 and 3.19 J/cm^2, respectively, which decreases by 40.2%. It could be considered that the decrease of LIDT is related to the color centers and the defects or helium bubbles induced by helium implantation.

To investigate the surface morphology evolution of sapphire after laser radiation, the samples are measured with optical microscope. The optical micrographs of laser damage before and after He implanted sapphire are shown in Fig. 8. It is clearly revealed that there are two different types of surface morphologies. Seen from Fig. 8(a), it is shown that the damage is a typical crater with many cracks around, which is similar to the damage morphology of fused slilica[25]. The inset in Fig. 8(a) is the profile of the damage crater, which shows that the maximum depth is about 12 μm. However, for the He-implanted sample, the damage area seems like lava eruption melted sapphire with many bubbles inside, which can be clearly observed from Fig. 8(b). It is probably due to the destruction of the crystal structure or helium bubble embedded in the near surface.

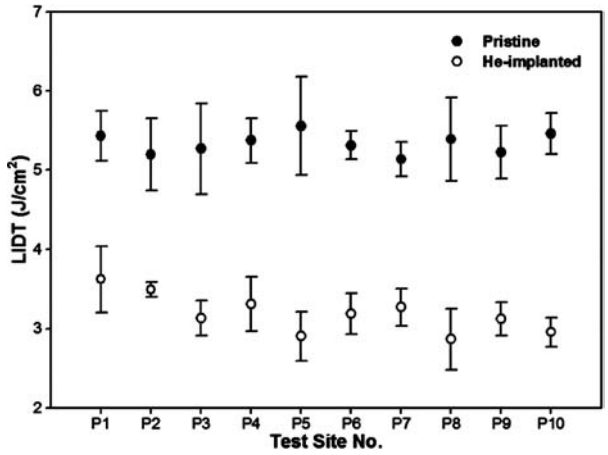

Fig. 7 – Distribution of LIDTs before and after He implanted sapphire

The mechanisms of laser-induced damage have been investigated by previous studies[26-28], including cold avalanche ionization, electron impact ionization, photo-ionization, thermal explosion and thermal diffusion. However, the thermal effect should be responsible for the laser-induced damage in the present work. After He ions implantation, not only the structure of single crystal has been destroyed, but also a large amount of defects and helium bubbles are produced near the surface. Therefore, the sapphire has lower melting point. It can be seen that the laser damage has changed from burst damage resulted from stress to melting damage induced by thermal effect.

Based on the results, the decrease of LIDT is mainly due to the strong absorption of color centers induced by the aggregation of defects. Because of the laser wavelength, 355 nm, is just in the absorption band centered at 360 nm. The absorption coefficient will increase when exposed to the laser pulse train and the lifetime of the induced absorption can be controlled by the duration of the exposure and the intensity[29]. In addition, the surface morphologies have been changed greatly due to the defects and helium bubbles after He ions implantation. It will inevitable degrade the laser damage resistance of the He-implanted samples. The decrease of damage threshold is also related to the surface morphologies.

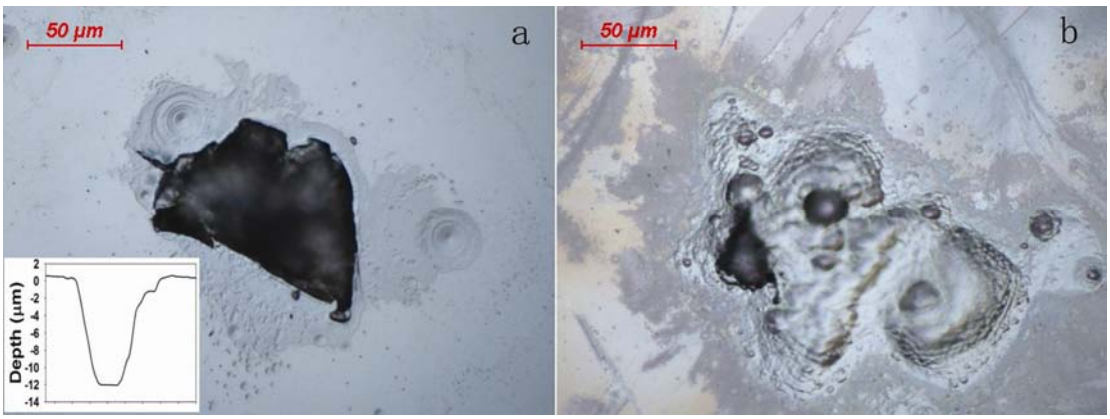

Fig. 8 – Optical micrographs of (a) laser damage before and (b) He implanted sapphire

Furthermore, the surface roughness and bubbles will decrease the damage threshold because the effective electric-field is changed[30]. It has been proved that the light modulation may cause the decrease of damage threshold[31,32]. Therefore, it is concluded that the color centers, surface morphologies and the light modulation are responsible for the remarkable degradation of laser damage resistance.

4. Conclusions

A uniform layer of He impurity in the range of 80-200 nm beneath the surface of sapphire is obtained by ion implantation with a series of energies. After He ions implantation, the defects and helium bubbles as well as lattice distortions are produced in the implantation area. As a consequence, the surface morphology of sapphire has been changed greatly. Two broad absorption bands are observed and their intensities significantly increase. An IR band shifts and obviously broadens. The laser damage tests show that the LIDT has decreased greatly after He ions implantation. The color centers, the surface morphologies and the light modulation are responsible for the remarkable degradation of laser damage resistance.

Acknowledgment

This study is supported financially by the NSAF Joint Foundation of China (Grant No.U1330103).

Reference

1 Izerrouken M, Meftah A & Berkani S, *Nucl Instru Methods B*, 326 (2014) 90.
2 Tanabe T, Fujiwara M & Miyazaki K, *J Nucl Mater*, 233–237, (1996) 1344.
3 Sakurai Y, Nagasawa K, Nishikawa H & Ohki Y, *J Appl Phys*, 86 (1999) 370.
4 León M, Martín P, Bravo D, López F J, Ibarra A, Rascón A & Mota F, *J Nucl Mater*, 374 (2008) 386.
5 Guo D C, Jiang X D, Huang J, Wang F R, Liu H J, Xiang X, Yang G X, Zheng W G & Zu X T, *Opt Express*, 22 (2014) 29020.
6 González de Vicente S M, Moroño A & Hodgson E R, *J Nucl Mater*, 417 (2011) 790.
7 Jardin C, Canut B & Ramos S M M, *J Phys D:Appl Phys*, 29 (1996) 2066.
8 Xiang X, Zu X T, Zhu S & Wang L M, *Appl Phys Lett*, 84 (2004) 52.
9 Xiang X, Zu X T, Zhu S, Wei Q M, Zhang C F, Sun K & Wang L M, *Nanotechnol*, 17 (2006) 2636.
10 Xiang X, Zu X T, Zhu S, Wang L M, Shutthanandan V, Nachimuthu P & Zhang Y, *J Phys D- Appl Phys*, 41 (2008) 225102.
11 Townsend P D, *Rep Prog Phys*, 50 (1987) 501.
12 Ziegler J F, Ziegler M D & Biersack J P, *Nucl Instru Methods B*, 268 (2010) 1818.
13 Crunteanu A, Jänchen G, Hoffmann P, Pollnau M, Buchal C, Petraru A, Eason R W & Shepherd D P, *Appl Phys A*,76 (2003) 1109.
14 González de Vicente S M, Morono A & Hodgson E R, *Fusion Sci Technol*, 56 (2009) 125.
15 Zinkle S J, *Nucl Instru Methods B*, 286 (2012) 4.
16 Van Huis M A, van Veen A, Labohm F, Fedorov A V, Schut H, Kooi B J & De Hosson J T M, *Nucl Instru Methods B*, 216 (2004) 149.
17 Sasajima N, Matsui T, Furuno S, Hojou K & Otsu H, *Nucl Instru Methods B*, 148 (1999) 745.
18 Zinkle S J & Kinoshita C, *J Nucl Mater*, 251 (1997) 200.
19 Jiang Y, Xiang X, Wang H J, Yuan X D, He S B, Lv H B, Zheng W G & Zu X T, *Opt Laser Technol*, 44 (2012) 948.
20 Izerrouken M & Benyahia T, *Nucl Instru Methods B*, 268 (2010) 2987.
21 Abdukadyrova I K, *Inorg Mater*, 44 (2008) 721.
22 Pechar F, *Cryst Res Technol*, 20 (1985) 239.
23 Evans B D & Stapelbroek M, *Phys Rev B*, 18 (1978) 7089.
24 Lee K H & Crawford J H, *Phys Rev B*, 19 (1979) 3217.
25 Dai W, Xiang X, Jiang Y, Wang H J, Li X B, Yuan X D, Zheng W G, Lv H B & Zu X T, *Opt Laser Eng*, 49 (2011) 273.
26 Deng H X, Zu X T, Xiang X & Sun K, *Phys Rev Lett*, 105 (2010) 113603.
27 Manenkov A A, *Opt Eng*, 53 (2014) 010901.
28 Yu J X, Xiang X, He S B, Yuan X D, Zheng W G, Lv H B & Zu X T, *Adv Cond Matter Phys*, 2014 (2014) 10.
29 Zhang X R, Emmert L A & Rudolph W, *Appl Opt*, 52 (2013) 8245.
30 Bloembergen N, *Appl Opt*, 12 (1973) 661.
31 Zhong M, Yang L, Ren W, Xiang X, Liu X, Lian Y Y, Xu S Z, Guo D C, Zheng W G & Yuan X D, *Acta Phys. Sin -Ch Ed*, 63 (2014) 246103.
32 Hua J R, Li L, Xiang X & Zu X T, *Acta Phys Sin -Ch Ed*, 60 (2011) 237.